# POST-IRRADIATION EXAMINATIONS OF HIGH-BURNUP PWR FUEL RODS – INITIAL RESULTS

BRUCE BEVARD,[1] ROSE MONTGOMERY,[1] JOHN M. SCAGLIONE[1]
*[1]Used Fuel Systems Group, Oak Ridge National Laboratory, Oak Ridge, TN 37831*
*865-574-0279 and bevardbb@ornl.gov*

## ABSTRACT

The High-Burnup Spent Fuel Data Project (herein referred to as the "project"), sponsored by the US Department of Energy (DOE) Office of Nuclear Energy (NE), is focused on experimentally evaluating the effects of long-term storage and transportation on high-burnup (HBU) (defined as >45 gigawatt days per metric ton uranium) pressurized water reactor (PWR) spent nuclear fuel (SNF). To support this project, in the fall of 2017 an instrumented bolted-lid cask (project cask) at the North Anna reactor site was loaded with intact, HBU PWR fuel assemblies (project assemblies) having four different kinds of cladding. This cask will be reopened in approximately 10 years for inspection. To support pre- and post-storage SNF rod characterization, 25 "sister rods" similar to the rods being stored in the project cask were extracted from seven different fuel assemblies at the North Anna nuclear power plant for post-irradiation examination (PIE).

The sister rod testing program has multiple objectives, including the following.

(1) Baseline testing will be conducted to provide essential information on the physical condition and properties of the cladding and the fuel in the cladding prior to the loading, drying, and long-term dry storage process (analogous to an experiment control group). At the end of the 10 year dry storage period, similar tests are expected to be performed on the fuel rods extracted from the cask to identify any changes in the properties of the rods that may have occurred.

(2) Accelerated separate effects tests (SETs) and small-scale tests (SSTs) will be conducted to provide material property and physical data to explore a wide range of conditions that may occur in other dry storage systems and/or while the fuel is being transported after aging.

All nondestructive examinations (NDE) have been completed and destructive tests began in early 2018. Destructive testing will be focused on understanding overall SNF rod strength and durability for both composite fuel and defueled cladding to support existing fuel storage licensing and future transportation. This paper presents the key NDE observations obtained from the sister rod examinations to date and describes some of the planned measurements, equipment, and procedures that will be implemented for the initial set of destructive examinations.

**Keywords: dry storage, spent nuclear fuel, high burnup, sister rods, SNF, material properties**

## 1. Introduction

The sister rods are expected to provide a very good representation of the initial condition of all HBU spent nuclear fuel rods in dry storage since they are within the top 10 percentile of burnups for all commercial spent nuclear fuel stored in the United States. Fifteen of the 25 sister rods fall within the top 2 percentile of all US SNF burnups [1]. Detailed characterization of the sister rods, including nondestructive examinations (NDEs) and destructive examinations (DEs), will provide valuable baseline data supporting extended SNF dry storage and subsequent transport and will inform the safety bases for those activities. The ORNL sister rod test plan provides a detailed description of the examinations to be completed [2]; due to space limitations, this paper reflects only part of the NDE results collected to date. The results of all examinations to date are summarized by Morris [3] and Montgomery [4].

The sister rods include four different types of cladding materials: M5® (9 rods), ZIRLO® (12 rods), Zircaloy-4 (2 rods), and low-tin Zircaloy-4 (2 rods). The sister rods are fueled with $UO_2$ pellets with similar initial enrichments ranging from 3.59 to 4.55 wt% U-235. The parent assembly average burnups range from 50.0 to 57.9 GWd/MTU, with cooling times ranging from 7.1 to 28.7 y.

All 12 of the ZIRLO®-clad rods are the Westinghouse North Anna Improved Fuel Assembly design with Performance+ features (NAIF/P+Z); the 9 M5®-clad rods are AREVA's Advanced Mark-BW design; the 2 Zircaloy-4 (Zirc-4)-clad rods are the Westinghouse low-parasitic (LOPAR) fuel assembly design; and the 2 low-tin Zircaloy-4 (LT Zirc-4)-clad rods are the Westinghouse North Anna Improved Fuel Assembly design (NAIF). Thus, 16 rods are Westinghouse designed and manufactured and 9 rods are AREVA designed and manufactured [2].

In addition to the sister rod program's NDE scope, an additional radiation scanning project using a high-purity germanium gamma scanner (HPGe) was performed for the National Nuclear Security Administration (NNSA) and completed using the sister rods [5,6]. Also, a specialized eddy current examination for measurement of cladding hydrogen content was performed on 19 of the 25 sister rods by the Electric Power Research Institute (EPRI) as summarized by Montgomery [4] and were in line with the NDE results reported herein.

## 2. NDE Results

All the rods were examined nondestructively using ORNL's Advanced Diagnostics and Evaluation Platform (ADEPT), as shown in Fig. 1. The NDE on each rod included a complete visual inspection, gamma scanning, rod dimensional measurements, and eddy current measurements to locate cladding flaws (such as cracks or through-wall corrosion) and to estimate the oxide and cladding wall thickness. The rods were not brushed prior to these examinations.

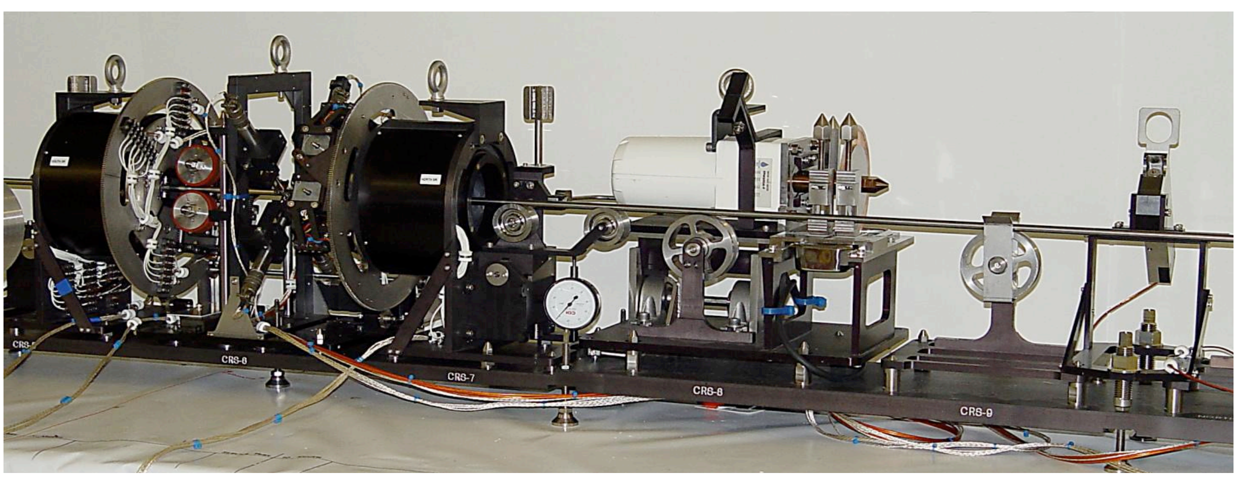


Fig 1. ORNL's ADEPT Spent Fuel Rod Handling and Measurement System.

## 2.1 General Condition and Visual Inspections

Montgomery [4] provides a summary of the general condition and visual inspections of the sister rods. The waterside surfaces of the rods were photographed extensively and collages of the 25 rods were assembled. Fig. 2 to Fig. 7 provide typical visible features by cladding alloy type. While the images were obtained using color photography, the primary coloration of the rods is grayscale. It should be noted that many of the figures show 360° images collaged from 8 images taken at 45° rod rotations of a 40 mm section the rod (as if the rod were cut axially and flattened). The darker stripes in the images result from radial light reflection at the top and bottom of the rod. There is a marked difference in the surface oxide appearance from alloy to alloy. All rods appear to be intact—no weld failures, obvious cladding breaches, or other significant defects were observed. Visual inspection indicated that grid-to-rod fretting (GTRF) marks are common on the sister rods. Rod insertion (pre-irradiation) and rod removal from the parent fuel assembly produced long axial scratches on most rods. Interactions with grid springs and dimples may have scraped off Chalk River unidentified deposits (CRUD) or oxides along the length of the rods during assembly removal at the orthogonal grid spring locations.

### 2.1.1 M5-clad sister rods

The M5 rods appear to have a matte black corrosion film with circular patches of thin oxide (confirmed by eddy current), as shown in Fig. 2(a). In some cases, the circular patches appear to have a peeling center; in others, the circular patches appear to have nucleated at grid spring contact locations and light fretting marks are visible at the center, as shown in Fig. 2(b).

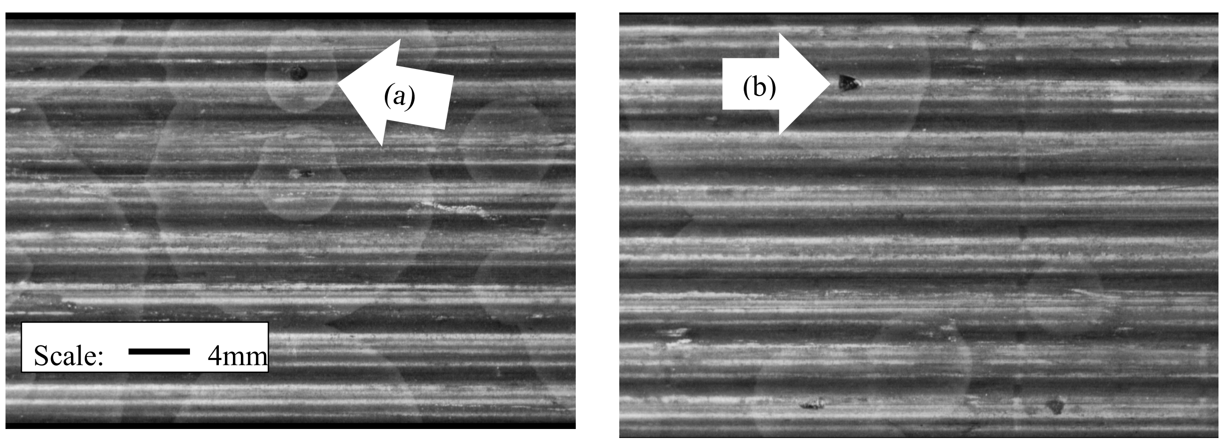


*Note: each image is a collage from a single rod derived from 8 images taken at 45° rod rotations to provide a flattened 360° image of a 40 mm section.*

Fig 2. Typical waterside surface appearance of all M5-clad sister rods where there is no apparent CRUD. All M5® rods appear to have a uniform matte black oxide layer, with the appearance of heavier oxidation in circular patches, which in some cases (a) have begun to peel at the center or (b) appear to have nucleated at light fretting marks from grid spring contact.

Some shallow GTRF marks are visible, along with rod removal scratches. Some localized areas (mainly the lower elevations) of the M5 rods have thin CRUD layers, giving the appearance of a flaky thin skin, as shown in Fig. 3. Most of the M5 rods have shallow-to-moderate GTRF marks at the axial locations corresponding to the spacer grid elevations.

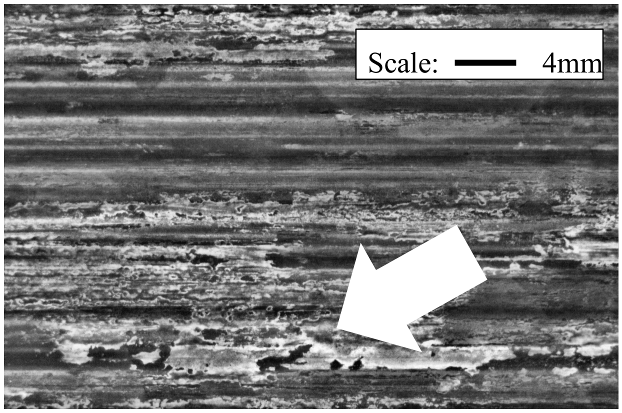


*Note:the image is a collage from 8 images taken at 45° rod rotations to provide a flattened 360° image of a 40 mm section.*

Fig 3. Localized flaky CRUD at 480 mm elevation on M5® cladding.

### 2.1.2 ZIRLO-clad sister rods

The ZIRLO-clad rods have a moderate-to-heavy oxide layer, as characterized by a silvery white coloration, with some oxide peeling/spalling observed, as shown in Fig. 4. GTRF marks are present on most rods and range in severity from shallow to deep, and rod insertion/removal scratches are visible. Figure 5 illustrates these details. No visible signs of through-wall cladding damage were observed.

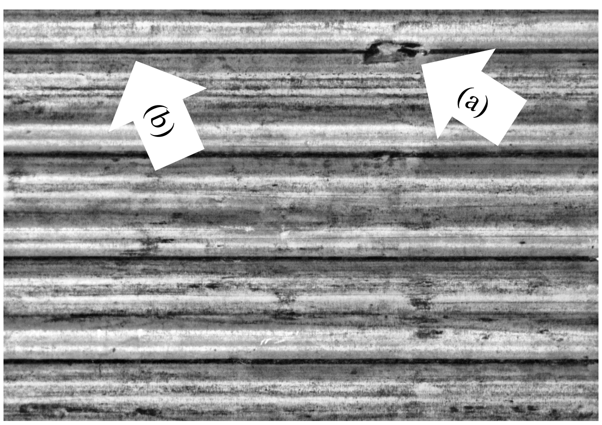


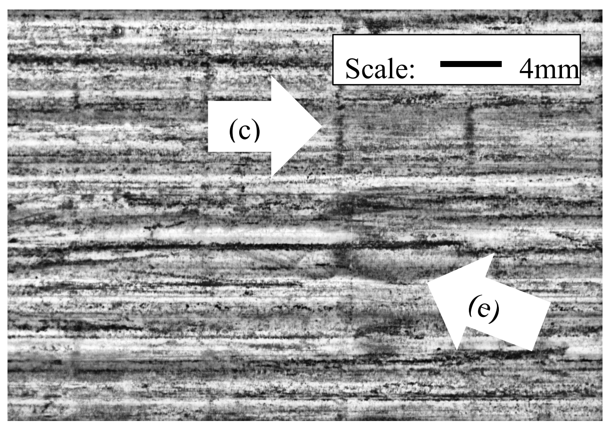


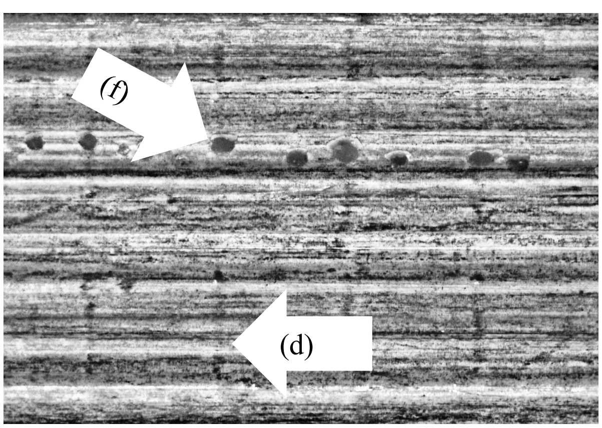


Fig 4. Typical waterside surface appearance of all ZIRLO-clad sister rods. The ZIRLO rods have a wavy silvery finish indicative of a moderate-to-heavy oxide layer. (a) moderate-to-deep grid-to-rod fretting marks and (b) deep rod removal axial scratches, (c and d) pellet-pellet interfaces visible as darker circumferential lines, (e) flow patterning visible at the exit side of spacer grid locations, and (f) oxide peeling.

*Note: each image is a collage from a single rod derived from 8 images taken at 45° rod rotations to provide a flattened 360° image of a 40 mm section.*

### 2.1.3 Zirc-4- and LT Zirc-4-clad sister rods

The Zirc-4 and LT Zirc-4 rods had the heaviest amount of oxide buildup/spalling, as shown in Fig. 5. No visible signs of through-wall damage or large areas of clad degradation were found in any of the rods. CRUD was observed on several of these rods, as shown in Fig. 6. The pellet-pellet interfaces are frequently visible in the images as circumferential dark stripes. Gaps at pellet-pellet interfaces (i.e., axial separation between one pellet and the next) are even more visible, as illustrated by the 3 mm gap shown in Fig. 5(b) confirmed with gamma scanning. During in-reactor operation, cladding at the pellet-pellet interface is slightly cooler. Hydrogen is known to migrate to cooler regions, while oxidation is expected to be reduced. While it is theorized that the combination of these effects creates the observed band of deeper coloration at the pellet-pellet interfaces, the difference in oxide thickness at these locations could not be confirmed with eddy current due to the increased pellet diameter at the pellet ends related to differential pellet swelling (also known as “bambooing”). Metallography will be used to check the local variation in hydride density and oxide thickness at some of the more prominent dark stripes.

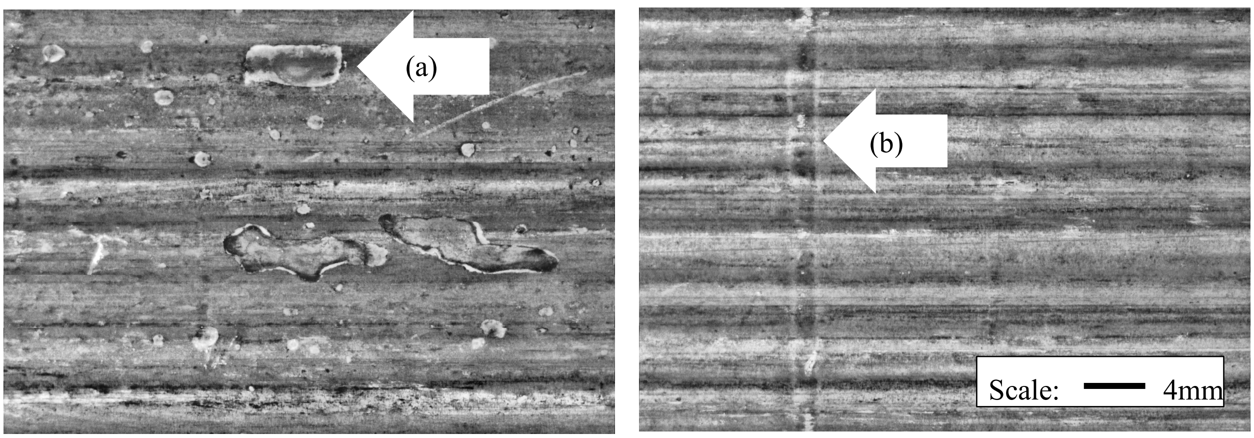


*Note: each image is a collage from a single rod derived from 8 images taken at 45° rod rotations to provide a flattened 360° image of a 40 mm section.*

Fig 5. Typical waterside surface appearance of Zirc-4-clad sister rods and LT Zirc-4-clad sister rods. The Zirc-4-clad rods have a wavy silvery surface finish indicative of a moderate-to-heavy oxide layer with (a) large areas of spalling in the higher power elevations and (b) a circumferential band indicative of a potential gap at a pellet-pellet interface.

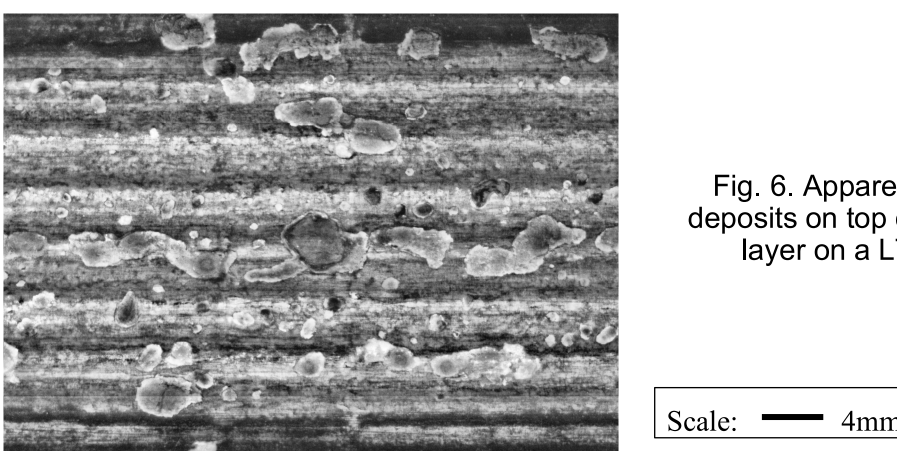


Fig. 6. Apparent flaky CRUD deposits on top of a heavy oxide layer on a LT Zirc-4 rod.

*Note: the image is a collage rod derived from 8 images taken at 45° rod rotations to provide a flattened 360° image of a 40 mm section.*

## 2.2 Gamma Scanning and Length Measurement Results

Morris [3] summarizes the results of the sister rod gamma scanning and length measurements. One-dimensional gamma scanning was conducted using a sodium iodide detector on all 25 rods in 2 energy ranges: 400 to 800 keV for examination of the fuel stack and 1,100 to 1,600 keV for examination of the structural components were used to measure relative gamma activity as a function of axial position, note any burnup depressions at spacer grid elevations, determine pellet stack height, and note any gaps between pellets. The gamma scans were also used to specify cutting locations for DE specimens. Data were collected in 1 mm increments along the axis of the sister rods, indexed to the bottom of the rod. Fig. 7 provides an example of the data taken during the gamma scan and the information derived from it. More detailed descriptions are provided by Morris [3] and Montgomery [4]. Assuming the initial pellet stack length was 144 inches [7], pellet stack growth can be estimated, as shown in Table 1.


Fig 7. An example of the data taken during a gamma scan. A reduction in burnup at the spacer grid locations results in a depression in the number of counts detected. The detector is sensitive enough to reflect drop-in counts related to the pellet-pellet interfaces (as shown in the yellow trace).

Gamma scans allow for differentiation of every pellet in the rod because the pellet dish and chamfer regions are large enough to provide a significant drop in gamma source term. Because each pellet is visible, axial gaps in the stack can also be observed. Seventeen stack gaps were observed in the 25 sister rods, with the largest gap estimated as 5 mm long.

### 2.2.1 Rod Diameter Measurements

Linear Variable Differential Transformer (LVDT) profilometry measurements on the sister rods were completed in April 2017. Two pairs of LVDTs were used: LVDT-1 and LVDT-2 measured 45° off the horizontal plane, and LVDT-3 and LVDT-4 measured 45°off the vertical plane. The two sets of measurements are 90° apart and can provide information on the extent to which the rod is out of round (ovality). The LVDT pairs are slightly offset axially for clearance. Using the LVDTs, the rods can only be measured to within about 200 mm of the end caps due to limitations of the rod-guiding mechanics. A 0.02 mm target accuracy of the LVDT apparatus was achieved. Calibration rods were used to calibrate the LVDTs and to check for accuracy. For the sister rod measurements, one pair of LVDTs (3 and 4) consistently read slightly low, so a correction was applied post-measurement. Table 3 provides a summary of the measured rod diameters of the sister rods. In general, the LT Zirc-4 and Zirc-4 rods had larger diameters than the M5 and ZIRLO rods at the same burnup; however, the Zirc-4 rods were expected to have more oxide and larger rod diameters, as they were lead test rods and were operated for four cycles instead of the typical three cycles. Using the gamma scanning plenum length measurement [3,4] with the rod diameter measured in the plenum region [4] and considering the oxide thickness measured using eddy current [4], the free plenum volume of each sister rod (neglecting the plenum spring volume and any free volume in the pellet stack) can be estimated. The results of these estimates are shown in Table 2.

Tab 1: Estimated pellet stack total growth grouped by rod type, assuming a typical 144 in. beginning of life stack height [7]

| **Cladding type** | **Sister Rod ID** | **Estimated pellet stack growth** | **Cladding type** | **Sister Rod ID** | **Estimated pellet stack growth** | **Cladding type** | **Sister Rod ID** | **Estimated pellet stack growth** |
|---|---|---|---|---|---|---|---|---|
| M5 | 30AE14 | 0.45% | ZIRLO | 6U3O05 | 0.50% | Zirc-4 | F35K13 | 0.89% |
| | 30AK09 | 0.59% | | 6U3I07 | 0.61% | | F35P17 | 1.13% |
| | 30AD05 | 0.53% | | 6U3M03 | 0.67% | Low Tin Zirc-4 | 3A1B16 | 0.61% |
| | 30AG09 | 0.45% | | 6U3M09 | 0.48% | | 3A1F05 | 0.72% |
| | 30AP02 | 0.59% | | 6U3K09 | 0.59% | | | |
| | 5K7C05 | 0.61% | | 6U3L08 | 0.69% | | | |
| | 5K7K09 | 0.48% | | 6U3P16 | 0.59% | | | |
| | 5K7O14 | 0.72% | | 3F9D07 | 0.72% | | | |
| | 5K7P02 | 0.56% | | 3F9N05 | 0.64% | | | |
| | | | | 3F9P02 | 0.64% | | | |
| | | | | 3D8B02 | 0.69% | | | |
| | | | | 3D8E14 | 0.80% | | | |

Tab 2: Estimated rod plenum free volume (neglecting the plenum spring volume and any free volume in the pellet stack) grouped by rod type

| **Cladding type** | **Sister Rod ID** | **Estimated rod plenum free volume (cc)** | **Cladding type** | **Sister Rod ID** | **Estimated rod plenum free volume (cc)** | **Cladding type** | **Sister Rod ID** | **Estimated rod plenum free volume (cc)** |
|---|---|---|---|---|---|---|---|---|
| M5 | 30AE14 | 9.36 | ZIRLO | 6U3O05 | 9.19 | Zirc-4 | F35K13 | 8.94 |
| | 30AK09 | 9.09 | | 6U3I07 | 8.90 | | F35P17 | 8.70 |
| | 30AD05 | 9.40 | | 6U3M03 | 9.03 | Low Tin Zirc-4 | 3A1B16 | 9.67 |
| | 30AG09 | 9.46 | | 6U3M09 | 9.29 | | 3A1F05 | 9.43 |
| | 30AP02 | 9.14 | | 6U3K09 | 9.11 | | | |
| | 5K7C05 | 9.18 | | 6U3L08 | 8.85 | | | |
| | 5K7K09 | 9.42 | | 6U3P16 | 9.12 | | | |
| | 5K7O14 | 8.99 | | 3F9D07 | 8.80 | | | |
| | 5K7P02 | 9.26 | | 3F9N05 | 9.03 | | | |
| | | | | 3F9P02 | 9.03 | | | |
| | | | | 3D8B02 | 8.87 | | | |
| | | | | 3D8E14 | 8.84 | | | |

Tab 3: Summary of sister rod outer diameter measurements

| Sister Rod | Alloy | Rod maximum OD (mm) | Rod minimum OD (mm) | Rod average OD (mm) |
|---|---|---|---|---|
| 30AD05 | M5 | 9.50 | 9.38 | 9.43 |
| 30AE14 | | 9.50 | 9.41 | 9.45 |
| 30AG09 | | 9.52 | 9.42 | 9.46 |
| 30AK09 | | 9.51 | 9.42 | 9.46 |
| 30AP02 | | 9.51 | 9.41 | 9.45 |
| 5K7C05 | | 9.49 | 9.40 | 9.46 |
| 5K7K09 | | 9.49 | 9.40 | 9.45 |
| 5K7O14 | | 9.51 | 9.41 | 9.46 |
| 5K7P02 | | 9.51 | 9.39 | 9.45 |
| 3D8B02 | ZIRLO | 9.52 | 9.42 | 9.46 |
| 3D8E14 | | 9.54 | 9.43 | 9.49 |
| 3F9D07 | | 9.51 | 9.42 | 9.46 |
| 3F9N05 | | 9.52 | 9.43 | 9.47 |
| 3F9P02 | | 9.50 | 9.41 | 9.44 |
| 6U3I07 | | 9.55 | 9.42 | 9.45 |
| 6U3K09 | | 9.52 | 9.42 | 9.47 |
| 6U3L08 | | 9.51 | 9.41 | 9.45 |
| 6U3M03 | | 9.52 | 9.42 | 9.46 |
| 6U3M09 | | 9.55 | 9.41 | 9.47 |
| 6U3O05 | | 9.52 | 9.41 | 9.46 |
| 6U3P16 | | 9.52 | 9.38 | 9.45 |
| 3A1B16 | LT Zirc-4 | 9.59 | 9.40 | 9.47 |
| 3A1F05 | | 9.63 | 9.36 | 9.49 |
| F35K13 | Zirc-4 | 9.61 | 9.41 | 9.49 |
| F35P17 | | 9.63 | 9.44 | 9.52 |

## 2.3 Eddy Current Exams

Eddy current measurements were used to estimate the waterside oxide thickness. Eddy current lift-off measurements use a contact probe to measure the distance from the probe tip to the electrically conductive surface (the fuel rod cladding), as illustrated in Fig. 8. The measurement includes the thickness of any nonconductive surfaces between the probe tip and the cladding, including oxide, CRUD, and foreign material. Spalling oxide indicates a thinner lift-off, especially if measurement averaging techniques are used in the data processing. The eddy current technique relies heavily on calibration using an unirradiated cladding alloy with known lift-off examples. Three calibration standards were used for the sister rod measurements—one M5, one ZIRLO, and one Zirc-4—using unirradiated cladding materials. Magnetic deposits such as those frequently encountered in boiling water reactor (BWR) rods are known to produce overestimates of the lift-off, and the absence of magnetic CRUD on the sister rods was verified using magnets to impose saturated conditions and monitoring for signal changes. The maximum measured lift-off for each sister rod is provided in Table 4. While the M5 and ZIRLO fuel rods had lift-off measurements that were consistent with previously reported oxidation thickness values [7], the Zirc-4 and LT

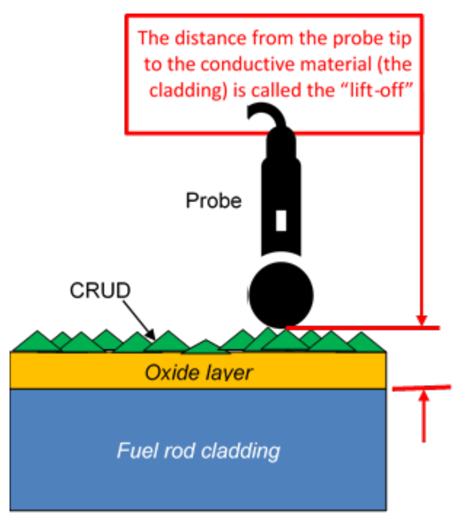


Fig 8. Schematic of eddy current test

Zirc-4 lift-off values were higher than expected [based on 8] and likely include a fairly large thickness of CRUD. Metallographic examinations will be used to confirm the oxide and CRUD thicknesses.

Tab 4: Summary of sister rod lift-off measurements

| Sister Rod | Cladding Alloy | Maximum rod average measured lift-off (μm)[a] | Elevation of maximum rod average measured lift-off (mm)[b] | Axial peak measured lift-off (μm)[c] | Elevation of axial peak measured lift-off (mm)[d] |
|---|---|---|---|---|---|
| 30AD05 | M5 | 20 | 3245 | 21 | 3245 |
| 30AE14 | | 27 | 3445 | 31 | 3445 |
| 30AG09 | | 20 | 3405 | 23 | 3225 |
| 30AK09 | | 16 | 3425 | 20 | 3865 |
| 30AP02 | | 18 | 3465 | 22 | 3705 |
| 5K7C05 | | 17 | 3365 | 22 | 3545 |
| 5K7K09 | | 20 | 3405 | 21 | 3405 |
| 5K7O14 | | 19 | 3435 | 22 | 3355 |
| 5K7P02 | | 18 | 3445 | 19 | 3465 |
| 3A1B16 | LT Zirc-4 | 138 | 3135 | 149 | 3135 |
| 3A1F05 | | 164 | 3115 | 185 | 3105 |
| 3D8B02 | ZIRLO | 36 | 3145 | 41 | 3105 |
| 3D8E14 | | 64 | 3205 | 72 | 3165 |
| 3F9D07 | | 69 | 3115 | 87 | 3255 |
| 3F9N05 | | 65 | 3075 | 85 | 3115 |
| 3F9P02 | | 33 | 3175 | 41 | 3235 |
| 6U3I07 | | 29 | 3085 | 32 | 3465 |
| 6U3K09 | | 38 | 3135 | 42 | 3255 |
| 6U3L08 | | 47 | 3245 | 62 | 3245 |
| 6U3M03 | | 50 | 3165 | 60 | 3195 |
| 6U3M09 | | 48 | 3125 | 53 | 3305 |
| 6U3O05 | | 62 | 3165 | 66 | 3245 |
| 6U3P16 | | 35 | 3175 | 44 | 3155 |
| F35K13 | Zirc-4 | 141 | 3085 | 156 | 3045 |
| F35P17 | | 150 | 3055 | 161 | 3085 |

[a]For the maximum average measured lift-off, the four-quadrant data is averaged individually over 10 mm elevation intervals, and then the four quadrants are averaged. The maximum is the maximum observed for the whole rod. The lift-off is the sum of the oxidation layer and any CRUD present. Note that magnetic CRUD is not present, as verified by EPRI during their F-SECT examinations.

[b]The elevation reported is that corresponding to the location where the maximum average lift-off was measured.

[c]The reported peak is the maximum from any one of the quadrant average measured lift-offs. The data in each quadrant is averaged individually over 10 mm elevation intervals

[d]The elevation reported is that corresponding to the location where the peak average lift-off was measured for any single quadrant.

## 2.4 Rod Surface Temperature Measurements

Surface temperature measurements were taken intermittently over the course of a year. To eliminate the effects of the hot cell airflow, an isolation housing was fabricated using 3D printing, as shown in Fig. 9. The housing included a through-hole for rod insertion and a cavity for the U-shaped thermocouple probe. Using the isolation housing, the surface temperature of several rods was measured at the axial mid-plane over several days. The maximum temperature measured was 31.1°C, was similar for all rods measured, and was consistent with expectations. Although the temperature was observed to vary in the daytime hours, the variation was not significant and did not appear to correlate with outdoor conditions. Rather, it is likely that the variation was related to the times when the lights were on in the hot cell, as the lights in the cell produce quite a bit of heat. Measurements during a cycle of approximately 42 hours are shown in Fig. 10. Additionally, the surface temperatures of two rod locations in the storage array (with a rod inserted) were measured at the axial mid-plane over several weeks. Because the heat produced by individual fuel rods is quite low, the resulting temperature differential from ambient was small and difficult to monitor in the hot cell environment.

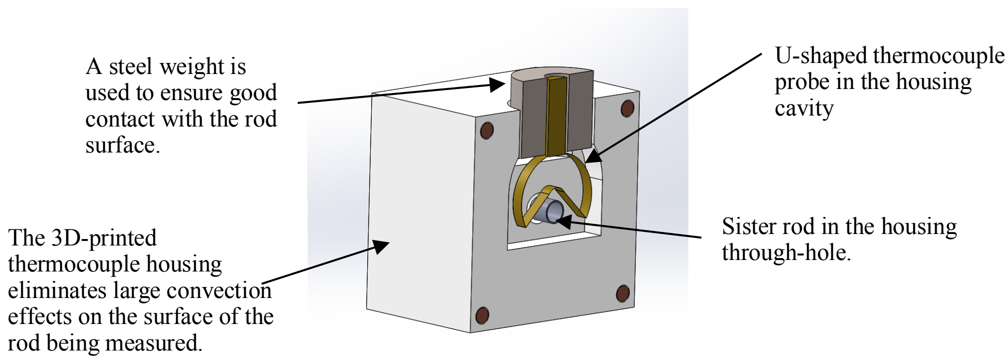


Fig 9. Cross-sectional view of the thermocouple isolation housing used to measure the surface temperature of selected sister rods.

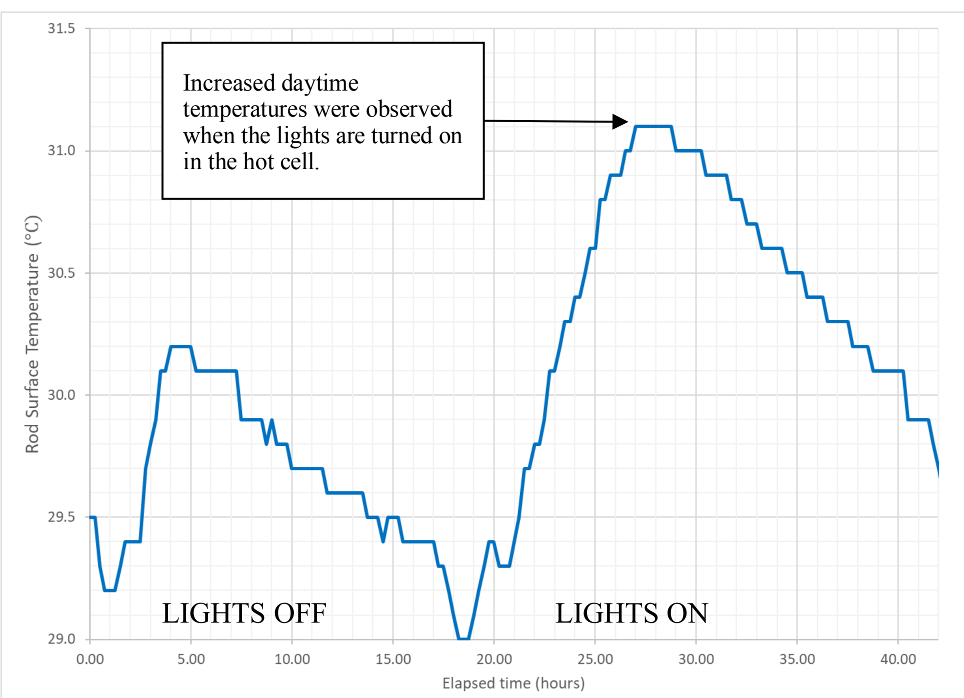


Fig 10. 42-Hour measurement of surface temperature of Sister Rod at the midplane, in the temperature housing and on the ADEPT (not in the storage array).

## 3. Conclusion

NDE of the 25 PWR spent fuel rods in the High-Burnup Spent Fuel Data Project is complete. The results of gamma scanning, length measurements, and visual examinations are available and provide detailed information on each rod, including axial burnup profile, average rod length, average pellet length, identification of pellet-pellet stack gaps greater than 1 mm in length, location of heavy and spalling oxide, location of GTRF marks, and location of CRUD. The results of the NDE will be used to identify the best locations for rod cutting, to select appropriate specimens for DE, and to provide data for code validation activities.

The DE will continue over the next few years and will include puncture, gas communcation testing, spiral notch torsion toughness (SNTT), cyclic reversible bending fatigue (CIRFT), four point bend, axial tension testing, microhardness, fueled and defueled ring compression testing, optical microscopy, and total hydrogen measurements.

## 4. References


[1] Scaglione, J. M., *A Unified Spent Nuclear Fuel Database and Analysis System*, International Conference on Management of Spent Nuclear Fuel from Nuclear Power Reactors: An Integrated Approach to the Back End of the Fuel Cycle, IAEA. 2015.

[2] Montgomery, R. A. et al., *Post-irradiation Examination Plan for High Burnup Demonstration Project Sister Rods*, SFWD-SFWST-2017-000090 ORNL/SR-2016/708, Oak Ridge National Laboratory, Oak Ridge, Tennessee. December 30, 2016.

[3] Morris, R. N. and R. A. Montgomery, *Sister Rod Nondestructive Examination Status Report (October – March) FY 2017*, SFWD-SFWST-2017-000089 ORNL/SR-2017/138, Oak Ridge National Laboratory, Oak Ridge, Tennessee. 2017.

[4] Montgomery, R. A. et al. *Sister Rod Nondestructive Examination Final Report*, SFWD-SFWST-2017-000003 ORNL Rev. 1/SPR-2017/484 Rev. 1, Oak Ridge National Laboratory, Oak Ridge, Tennessee. 2018.

[5] Susan Kane Smith, Stephen Croft, Andrew Nicholson, Greg Nutter, "High-resolution Gamma Spectroscopy Measurements of Pressurized Water Reactor Spent Nuclear Fuel Rods." ORNL/SPR-2017/535, January 2018.

[6] U.S. Nuclear Regulatory Commission, *0519 - R304P - Westinghouse Technology 3.1 Reactor Vessel and Internals* available at www.nrc.gov/docs/ML1122/ML11223A212.pdf.

[7] Halligan, J.R. et al., *PWR Fuel Performance and Key Developments in Material and Mechanical Design*, TopFuel 2015 Conference Proceedings, Zurich, Switzerland, 2015.

[8] Motta, A.T., *Corrosion of Zirconium Alloys Used for Nuclear Fuel Cladding*, Annual Reviews, 10.1146/annurev-matsci-070214-020951, 2015.